Table 1 Observational parameters

Date	Z (R_m)	$4\pi I$ (R)	v (km s^{-1})	φ (°)	γ	g (s^{-1})	$N_{tangent}$ (cm^{-2})
7 July 1998	2.25	384	7.561	79	0.14	10.46	3.67×10^7
19 July 1998	1.4	422	2.249	101	0.0352	2.29	1.8×10^8

The observational parameters, emission intensity, and derived Ca abundance for the selected emission spectra of Fig. 1. The radial distance, Z, is measured from the planet's centre to the tangent point of the line-of-sight to the observer in units of planetary radii (R_m); $4\pi I$ is the column emission intensity in Rayleighs (1 R) = 10^6 photons cm^{-2} s^{-1}); v is the velocity of the planet radial to the sun; φ is the Sun–Mercury–Earth phase angle; γ is the fraction of solar continuum at the line centre wavelength as seen by atoms at rest in Mercury's atmosphere; g is the scattering coefficient described in the text; and $N_{tangent}$ is the column abundance tangent to the line of sight.

energy[15,16]; therefore, the assignment of an equivalent temperature of 12,000 K probably underestimates the mean energy of the gas. This high temperature is expected for an ion-sputtered source[17], but is at least twice that expected from an impact vapour source[18], and ten times that expected from a photo-sputtered source[15]. The localization of Ca in the vicinity of the polar regions, if verified by subsequent observations, along with increased column abundance in the anti-solar direction, supports the hypothesis that the Ca in the atmosphere is sputtered by ions directed poleward by Mercury's magnetosphere. We note that the Ca–O bond strength is 4.8 eV, in contrast with 2.6 eV for the Na–O bond, so that Ca may be sputtered in a larger proportion bound as Ca–O than is the case for Na and Na–O.

The low-Ca zenith abundance (1.1×10^8 cm^{-2}) is much less than previous predicted (6.4×10^8 cm^{-2}, ref. 19) and observational upper limits (7.4×10^8 cm^{-2}, ref. 20). Although the refractory nature of Ca will limit is supply to the atmosphere, the observed low density and apparent polar concentration of Ca are consistent with a surface composition that is more volatile-rich than that of the Moon[19]. The recent identification of labrodorite feldspar, a 30%–50% Na-rich albite, on Mercury[21], along with other infrared observations[22], is additional evidence for a Ca-poor material. Alternatively, there may be patchy locations of Na-rich, K-rich (Ca-poor) materials[23]. □

Received 23 July; accepted 15 December 1999.

1. Goettel, K. A. in *Mercury* 613–621 (Univ. Arizona Press, Tucson, 1988).
2. Lewis, J. S. in *Mercury* 651–666 (Univ. Arizona Press, Tucson, 1988).
3. Lewis, J. S. Metal/silicate fractionation in the solar system. *Earth Planet Sci.* **15,** 286–290 (1992).
4. Potter, A. E. & Morgan, T. H. Discovery of sodium in the atmosphere of Mercury. *Science* **229,** 651–653 (1985).
5. Potter, A. E. & Morgan, T. H. Potassium in the atmosphere of Mercury. *Icarus* **67,** 336–340 (1986).
6. Sprague, A. L. *et al.* Distribution and abundance of sodium in Mercury's atmosphere, 1985–1988. *Icarus* **129,** 506–527 (1997).
7. Killen, R. M. & Morgan, T. H. Maintaining the Na atmosphere of Mercury. *Icarus* **101,** 293–312 (1993).
8. McGrath, M. A., Johnson, R. E. & Lanzerotti, L. J. Sputtering of sodium on the planet Mercury. *Nature* **323,** 694–696 (1986).
9. Yakshinskiy, B. V. & Madey, T. E. Photon-stimulated desorption as a substantial source of sodium in the lunar atmosphere. *Nature* **400,** 642–644 (1999).
10. Killen, R. M., Potter, A. E., Fitzsimmons, A. & Morgan, T. H. Sodium D2 line profiles: clues to the temperature structure of Mercury's exosphere. *Planet. Space Sci.* **47,** 1449–1458 (1999).
11. Vogt, S. S. *et al.* HIRES: the high-resolution echelle spectrometer on the Keck 10-m telescope. *Proc. S.P.I.E.* **2198,** 362 (1994).
12. Chamberlain, J. W. & Hunten, D. M. *Theory of Planetary Atmospheres* (Academic Press, Orlando, 1987).
13. Kurucz, R. L., Furenlid, I., Brault, J. & Testerman, L. *Solar Flux Atlas From 296 to 1300 nm, National Solar Observatory Atlas No. 1* (Harvard Univ. Press, Boston, 1984).
14. Cheng, A. F., Johnson, R. E., Krimigis, S. M. & Lanzerotti, L. J. Magnetosphere, exosphere and surface of Mercury. *Icarus* **71,** 430–440 (1987).
15. Madey, T. E., Yakshinsky, V. N., Ageev, V. N. & Johnson, R. E. Desorption of alkali atoms and ions from oxide surfaces: relevance to origins of Na and K atmospheres of Mercury and the Moon. *J. Geophys. Res.* **103,** 5873–5887 (1998).
16. Chamberlain, J. W. Spectral line profiles for a planetary corona. *J. Geophys. Res.* **81,** 1774–1776 (1976).
17. Elphic, R. C. *et al.* Lunar surface composition and solar wind-induced secondary ion mass spectrometry. *Geophys. Res. Lett.* **18,** 2165–2168 (1991).
18. Sugita, S., Schultz, P. H. & Adams, M. A. In situ temperature measurements of impact-induced vapor clouds with spectroscopic methods. *Proc. Lunar Planet. Sci. Conf.* **28,** 1393–1394 (1997).
19. Morgan, T. H. & Killen, R. M. A non-stoichiometric model of the composition of the atmospheres of Mercury and the Moon. *Planet. Space Sci.* **45,** 81–94 (1997).
20. Sprague, A. L., Koslowski, R. W. H., Hunten, D. M. & Grosse, F. A. An upper limit on neutral calcium in Mercury's atmosphere. *Icarus* **104,** 33–37 (1993).
21. Sprague, A. L., Nash, D. B., Witteborn, F. C. & Cruikshank, D. P. Mercury's feldspar connection: mid-IR measurements suggest plagioclase. *Adv. Space Res.* **19,** 1507–1510 (1997).
22. Jeanloz, R., Mitchell, D. L., Sprague, A. L. & dePater, I. Evidence for a basalt free surface on Mercury and implications for internal heat. *Science* **268,** 1455–1457 (1995).
23. Sprague, A. L., Schmitt, W. J. & Hill, R. E. Mercury: Sodium atmospheric enhancements, radar bright spots and surface features. *Icarus* **136,** 60–68 (1998).

Acknowledgements

The data presented here were obtained at the W.M. Keck Observatory, which is operated as a scientific partnership between the California Institute of Technology, the University of California and the National Aeronautics and Space Administration. The observatory was made possible by the generous financial support of the W.M. Keck Foundation. We are grateful to the WMKO Observing Assistants for their help while conducting the observations. R.M.K. acknowledges the support of a NASA grant.

Correspondence and requests for materials should be addressed to T.A.B. (e-mail: tbida@keck.hawaii.edu).

North–south geological differences between the residual polar caps on Mars

P. C. Thomas*, M. C. Malin†, K. S. Edgett†, M. H. Carr‡, W. K. Hartmann§, A. P. Ingersoll‖, P. B. James¶, L. A. Soderblom, J. Veverka* & R. Sullivan***

* *Center for Radiophysics and Space Research, Cornell University, Ithaca, New York 14853, USA*
† *Malin Space Science Systems, P.O. Box 910148, San Diego, California 92191, USA*
‡ *US Geological Survey, Menlo Park, California 94025, USA*
‖ *Division of Geological and Planetary Sciences, California Institute of Technology, Pasadena, California 91125, USA*
§ *Planetary Science Institute, Tucson, Arizona 85719, USA*
¶ *Department of Physics and Astronomy, University of Toledo, Toledo, Ohio 43606, USA*
** *US Geological Survey, Flagstaff, Arizona 86001, USA*

Polar processes can be sensitive indicators of global climate, and the geological features associated with polar ice caps can therefore indicate evolution of climate with time. The polar regions on Mars have distinctive morphologic and climatologic features: thick layered deposits, seasonal CO_2 frost caps extending to mid latitudes, and near-polar residual frost deposits that survive the summer[1,2]. The relationship of the seasonal and residual frost caps to the layered deposits has been poorly constrained[3,4], mainly by the limited spatial resolution of the available data. In particular, it has not been known if the residual caps represent simple thin frost cover or substantial geologic features. Here we show that the residual cap on the south pole is a distinct geologic unit with striking collapse and erosional topography; this is very different from the residual cap on the north pole, which grades into the underlying layered materials. These findings indicate that the differences between the caps are substantial (rather than reflecting short-lived differences in frost cover), and so support the idea of long-term asymmetry in the polar climates of Mars.

Data from the Mariner 9 and Viking missions established the distribution of the three basic polar units on Mars. Layered deposits centred approximately on the poles, consisting of unknown proportions of water ice and dust averaging 1,200 km across and up to 3 km in thickness[5], seasonal carbon dioxide (CO_2) frost caps that remove about 25% of the martian atmosphere, and residual summer caps of frost: water ice in the north, CO_2 in the south[6–8]. The northern residual cap is nearly coextensive with the layered deposits; the southern one is very much smaller in extent than the layered deposits. Mariner 9 and Viking images could not resolve the relation of the residual frost caps to the underlying layered deposits.

Images from the Mars Orbiter Camera (MOC) on the Mars Global Surveyor spacecraft, with pixel scales as good as 1.5 m (ref. 9; 30–50 times better than most previous images) now provide comparisons of the residual caps and layers in both polar deposits.

Images from the MOC show that the north-polar residual cap surface has a rough ablational topography of pits, cracks and some knobs (Fig. 1). The residual cap surface grades into exposures of layers (each typically 1–3 m thick) at the edges of dark lanes that expose the underlying layered deposits in low-slope cross-section[10,11] (Fig. 1c). Layers exposed in the dark lanes are commonly expressed as subtle ridges or troughs[12] on the slopes, and usually have a disaggregated appearance.

In contrast to the north, the south residual cap has distinctive erosional or collapse topography (Fig. 2) affecting four or more layers, each about two metres thick (determined from shadow measurements). The top surface of the upper layer has polygonal depressions suggestive of thermal contraction cracks (Fig. 2a). Circular and cycloidal depressions, individual troughs with varying curvatures and groups of nearly parallel troughs giving 'fingerprint' patterns are also observed.

These distinctive morphologies occur throughout, but only within the south residual cap as mapped by Viking in 1977 (ref. 13). Isolated examples of degraded depressions and ridges are found in a few locations outside the residual cap in the south-polar layered deposits, but are not readily assigned to versions of the forms seen on the residual cap. These areas of the layered deposits have been thermally modelled[14] as dust-covered and mechanically distinct from the residual cap. Exposed layers or unconformities in polar deposits in both hemispheres do not show the kind of relief found on the southern residual cap.

Thicknesses of layers in the south residual cap area are not much greater than that predicted for seasonal CO_2 deposition near the pole (0.5–1 m; refs 1 and 8); this similarity raises the possibility that the features might be short-lived. Images at 1.5 to 5 metres per pixel acquired over five (Earth) months of the southern spring show no changes in the topography. Dark markings observed by Mariner 9 in 1972 at 120 metres per pixel correlate with arcuate remnants of the upper layer imaged by MOC. The persistence of a few metres of relief, less than a kilometre wide, for 27 years (scarp retreat of less than a few metres per year) in an area where material has been removed over horizontal scales of tens of kilometres, suggests that these distinctive forms may have survived for more than 1,000 years. Patterned materials at the bases of scarps (not shown here) may suggest long periods of thermal cycling[15], which at polar latitudes is nearly all seasonal; thus modification of the aprons alone might span hundreds of years. There are no obvious impact craters with diameters greater than 100 m in the 550+ MOC images of the south residual cap with pixel scales less than 20 m. These images cover about 35% of ~48,000 km^2 of the residual cap accessible to MOC (to 87 S). The lack of craters suggests a crater retention age of less than 10^5 years, substantially less than the more than 10^7 years inferred for the southern layered deposits outside the residual cap[16,17].

The MOC images of the southern residual cap also indicate that coverage by the seasonal cap is either thin, nearly transparent[8], or both. Although there might be a small component similar to the CO_2 ice 'slabs' inferred for other parts of the seasonal cap[8], the upper surface of the residual cap has a very high albedo in the spring and shows albedo features indicative of differential defrosting of some areas. However, there are no thick accumulations of drifted snow, and the crispness of the topography viewed with solar elevation angles of only two degrees suggests less than a metre of seasonal covering within the residual cap area.

Images from MOC indicate the following sequence of events in the south-polar residual cap area: (1) Deposition of at least the four upper layers on a lower surface. (2) Sag in areas a few tens of metres to a few hundred metres across in a large fraction of the residual cap area. (3) Collapse over sags and lateral expansion of depressions,

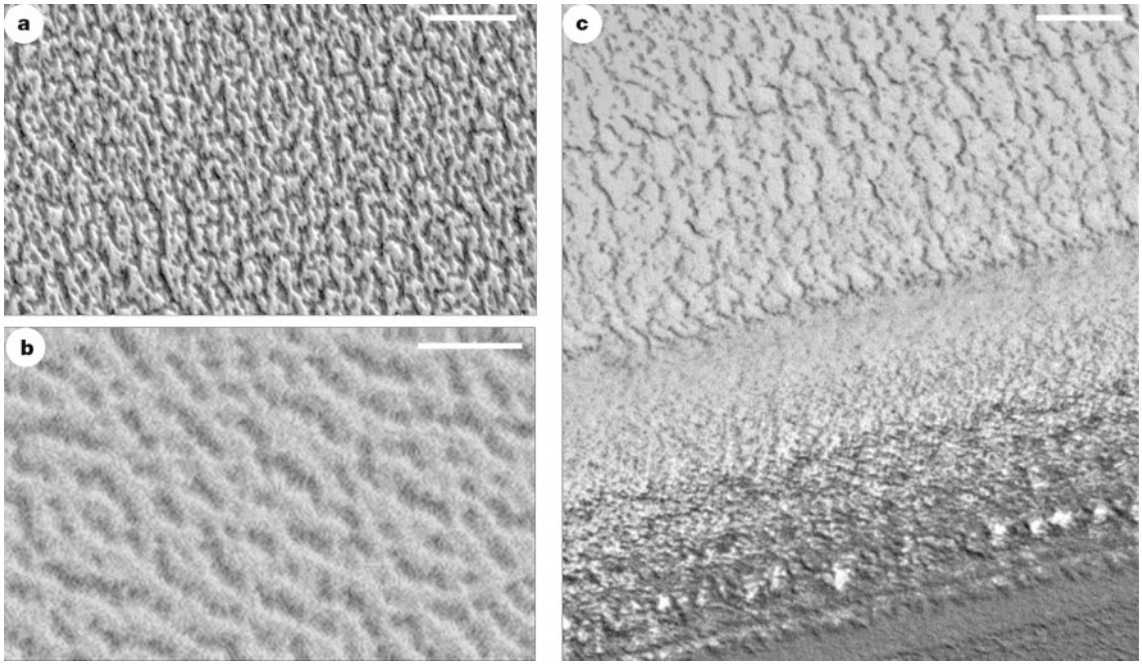

Figure 1 North-polar residual cap topography. **a**, Individual and connected pits in surface of residual cap. Portion of Mars Orbiter Camera (MOC) image M00-00547 (mapping phase 0, image 547), 82.1° N, 329.6° W, solar incidence angle $i = 73°$. Texture on most of the north-polar residual cap is a variant of pitting of approximately similar width depressions; length and connectivity of depressions varies. Depths inferred from minimal evidence of shadows are probably less than 2 m. Scale bar is 200 m. Illumination is from upper right. Aerocentric longitude of the sun (L_s) is 120° (0° is northern spring equinox). 5 April 1999. This and other images shown have been contrast enhanced. **b**, North-polar residual cap surface, portion of image CAL-00433; 86.9° N, 207.5° W; scale bar is 50 m. Illumination is from upper right. $L_s = 107°$. 8 March 1999. **c**, Merging of pits and fissures of residual cap topography with exposure of layers in walls of one of the dark lanes (troughs with wall slopes generally less than 10°) that traverse much of the northern layered deposits; area at bottom of image is largely frost-free. Portion of MOC image M00-02072; 85.9° N, 258.1° W; $i = 70°$. Scale bar is 100 m. Illumination is from upper right. $L_s = 124°$. 13 April 1999.

perhaps aided by insolation effects at the steeper parts of collapse depressions. (4) Removal of large areas of volatile materials leaving lag surfaces with less than 2 m of relief. (5) Formation of debris aprons around higher (9 m) scarps. (6) Production of moats around higher residual areas either by deposition of 1–2 m of material around debris aprons followed by loss of some apron material, or by further compaction of underlying materials by debris aprons and subsequent loss of some material from the debris aprons. (7) Further development of debris aprons, with a horizontal change of less than 20 m in scarp positions. Time scales associated with each specific step are unknown, although as noted above, the total time could greatly exceed 1,000 years.

Important features in the above sequence of events are the initial generation and form of collapse (sags), depression growth (possibly by sublimation), removal of large amounts of material (8 m by several thousand square kilometres) and a possible additional depositional period.

What causes the initial sags and collapse? The volume change at depth could be due to compaction or to removal of material. Compaction of layers that were anomalously porous might occur with further deposition in combination with heating owing to rising isotherms with increasing time of burial. The plan form of compacting material could reflect variations in thickness or texture of the original deposit, such as snow dunes. Removal of material would most probably be caused by sublimation of CO_2 or water ice. In either case, the collapse regime is apparently restricted to the area currently showing summer residual CO_2 at the surface. The circumstances suggest that CO_2 rather than water constitutes the collapsing unit. Carbon dioxide is the most likely constituent that could sublimate to initiate the sags because of its much higher vapour pressure and because of the apparent lack of collapse in areas of the water-ice-covered north-polar residual cap, or in the outlying south-polar layered deposits. That is, if water ice is the chief volatile constituent of the polar deposits[11], CO_2 deposits in the residual cap area would provide the contrast in volatility that the surface morphology suggests.

Although thick accumulations of CO_2 ice are probably not possible[18], a few metres of coverage could occur as they would have minimal basal pressure (0.6 MPa for 10 m of solid CO_2 ice) and would extract a very small fraction of the atmospheric CO_2

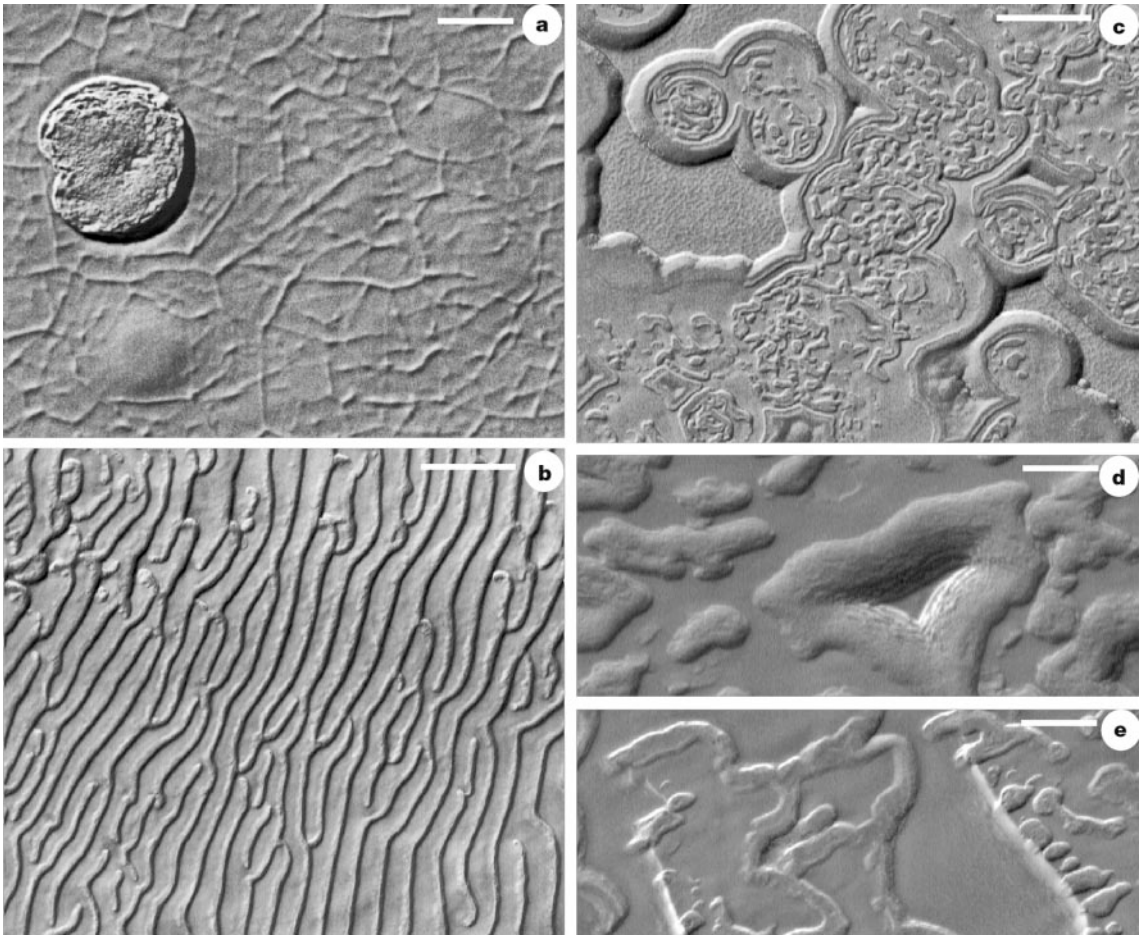

Figure 2 South-polar residual cap topography. **a**, Nearly circular depression and nearby sag surface on top layer. Polygonal cracks are prominent on undisturbed sections of the upper layer surface, but do not affect the margins of circular depressions. Portion of MOC image M09-00609; 87.0° S, 5.9° W; $i = 70°$. Scale bar is 100 m. Illumination is from lower right. $L_s = 237°$. 3 November 1999. **b**, 'Fingerprint' pattern of depressions. Elongated sags in other areas of residual cap suggest precursors of this topography. Steeper sides (right) of the troughs face in a more northerly direction, suggesting sublimation in expanding depressions, as with the more circular ones. Portion of MOC image M03-06756; 86.0° S, 53.9° W; $i = 88°$. Illumination is from lower right. Scale bar is 500 m. $L_s = 182°$. 4 August 1999. **c**, Circular collapse features, leaving mesas on upper surface with debris aprons and moats. Largest scarps here are about 4 m high. The uppermost layer is capable of supporting scarp slopes of ~20°; the aprons frequently have slopes of order 1°–3° (Fig. 2b); slopes are estimated from presence or absence of shadows as the sun gained elevation in the southern spring. Portion of MOC image M03-06646; 85.6° S, 74.4° W; $i = 88°$. Scale bar is 500 m. Illumination is from lower right. $L_s = 181°$. 3 August 1999. **d**, Residual mesa exposing four layers and surrounding moat. Formation of moats probably requires additional deposition and sublimation or compaction following removal of material from height of top layer exposed here. Portion of MOC image M07-02129; 86.9° S, 78.5° W; $i = 81°$. Scale bar is 100 m. Illumination is from bottom, right. $L_s = 204°$. 11 September 1999. **e**, Complex covering of depressions which suggest burial and exhumation of topography on part of the southern residual cap area. Portion of MOC image M04-03877; 84.6° S, 45.1° W, $i = 81°$, scale bar is 200 m. Illumination is from lower right. $L_s = 196°$. 29 August 1999.

reservoir. The removal of wide areas of the upper 8–10 m of the residual cap (Fig. 2c and d) after initial sag and collapse implies that most of those upper layers are also subject to sublimation, especially once the upper surface is fragmented or disturbed. Most of the eight metres that are removed is probably CO_2; the lag might be less volatile water ice. Radar data returns from the south-polar residual cap are very different from the north-polar cap[19], and can be interpreted as indicative of clean ice with large cavities.

The evolution of the topography after collapse (steps 4–7 above) suggests at least two subsequent non-steady-state periods. The wide area of removal of three or more layers (Fig. 2c and d) indicates considerable sublimation. The circular and near-circular forms may develop because at these high latitudes, ablational removal can become nearly azimuthally isotropic owing to the small change in solar elevation during the day. The remnant landforms suggest lag deposits from ablation and further collapse. The small proportion remaining as lag (Fig. 2a and c) suggests a small non-volatile (or less volatile) component in the upper layers of the residual cap area. The moats (Fig. 2c and d) also require some sequence of renewed deposition and subsequent partial removal, or a period of debris apron growth followed by apron retreat or compression of underlying layers. Additionally, some areas show probable burial and partial exhumation of the depressions (Fig. 2e).

The MOC data show that the southern residual cap is not simply a temporary anomaly of residual summer CO_2 frost; it is a geological feature indicative of depositional and ablational events recorded neither in the north nor in the outlying southern polar layered deposits. The geographical restriction to the CO_2 residual cap strongly suggests that CO_2 ice is involved, as does the apparent requirement for a component distinct from water ice. The most obvious environmental distinctions of the southern residual cap area are its elevation, about 6 km above the northern one[11,20], and its presence in the hemisphere that has very low atmospheric water content[2].

Indications of burial and exhumation (Fig. 2e, and steps 6 and 7 above) suggest repetitive, or even periodic formation of the distinctive southern residual cap morphology. Change in hemispheric asymmetry in polar processes has been attributed to periodic variations[21–24] in the orbital eccentricity, obliquity and season of perihelion of Mars. Even the shortest of these cycles, 51,000 years for season of perihelion, could easily allow the build-up (or sublimation) of the whole of the south residual cap unit. Eight metres of solid CO_2 accumulated as net residual in 1,000 years would require only about 2% of the current seasonal total[8] CO_2 to be retained each year. However, elucidation of the time scale represented by the residual deposits rests on detection of the net atmospheric CO_2 budget and on mapping cycles recorded in the layered deposits as a whole. □

Received 3 December 1999; accepted 7 January 2000.

1. James, P. B., Kieffer, H. H. & Paige, D. A. in *Mars* (eds Kieffer H., Jakosky, B., Snyder C. & Matthews, M.) 934–968 (Univ. Arizona Press, Tucson, 1992).
2. Jakosky, B. M. & Haberle, R. M. in *Mars* (eds Kieffer H., Jakosky, B., Snyder C. & Matthews, M.) 969–1016 (Univ. Arizona Press, Tucson, 1992).
3. Pollack, J. B., Colburn, D., Flasar, F. M., Kahn, R. Carlston, C. & Pidek, D. Properties and effects of dust particles suspended in the Martian atmosphere. *J. Geophys. Res.* **84,** 2929–2945 (1979).
4. Thomas, P. C., Herkenhoff, K., Howard, A. & Murray, B. in *Mars* (eds H. Kieffer, H., Jakosky, B., Snyder, C. & M. Matthews) 767–795 (Univ. Arizona Press, Tucson, 1992).
5. Smith, D. E. *et al.* The global topography of Mars and implications for surface evolution. *Science* **284,** 1495–1503 (1999).
6. Farmer, C. B., Davies, D. W. & LaPorte, D. D. Mars: Northern summer ice cap—water vapor observations from Viking 2. *Science* **194,** 1339–1340 (1976).
7. Kieffer, H. H. Mars south polar spring and summer temperatures. A residual CO_2 frost. *J. Geophys. Res.* **84,** 8263–8288 (1979).
8. Kieffer, H. H., Titus, T. N., Mullins, K. F. & Christiansen, P. R. Mars south polar spring and summer behavior observed by TES; seasonal cap evolution controlled by grain size. *J. Geophys. Res.* (submitted).
9. Malin, M. C. *et al.* Early views of the Martian surface from the Mars Orbiter Camera of Mars Global Surveyor. *Science* **279,** 1681–1685 (1998).
10. Howard, A. D., Cutts, J. A. & Blasius, K. R. Stratigraphic relationships within Martian polar cap deposits. *Icarus* **50,** 161–215 (1982).
11. Zuber, M. T. *et al.* Observations of the north polar region of Mars from the Mars Orbiter Laser Altimeter. *Science* **282,** 2053–2060 (1998).
12. Malin, M. C. & Edgett, K. S. The nature of layered outcrop expression in the martian polar layered terrains. *Lunar Planet. Sci.* **34,** Abstr. no. 1055 (2000).
13. James, P. B., Briggs, G., Barnes J. & Spruck, A. Seasonal recession of Mars' south polar cap as seen by Viking. *J. Geophys. Res.* **84,** 2889–2922 (1979).
14. Paige, D. A. & Keegan, K. D. Thermal and albedo mapping of the polar regions of Mars using Viking thermal mapper observations: 2. South polar region. *J. Geophys. Res.* **99,** 25993–26031 (1994).
15. Mellon, M. T. Small-scale polygonal features on Mars: Seasonal thermal contraction cracks in permafrost. *J. Geophys. Res.* **102,** 25617–25628 (1997).
16. Plaut, J. J., Kahn, R., Guinness, E. A. & Arvidson, R. E. Accumulation of sedimentary debris in the south polar region of Mars and implications for climate history. *Icarus* **76,** 357–377 (1988).
17. Herkenhoff, K. E. & Plaut, J. J. Surface ages and resurfacing rates of the polar layered deposits on Mars. *Icarus* (in the press).
18. Mellon, M. T. Limits on the CO_2 content of the martian polar deposits. *Icarus* **124,** 268–279 (1996).
19. Muhleman, D. O., Grossman, A. W. & Butler, B. J. Radar investigation of Mars, Mercury, and Titan. *Annu. Rev. Earth Planet. Sci.* **23,** 337–374 (1995).
20. Schenk, P. M. & Moore, J. M. Stereo topography of the south polar region of Mars: Volatile inventory and Mars landing site. *J. Geophys. Res.* (in the press).
21. Toon, O. B., Pollack, J. B., Ward, W., Burns, J. A. & Bilski, K. The astronomical theory of climatic change on Mars. *Icarus* **44,** 552–607 (1980).
22. Kieffer, H. H. & Zent, A. P. in *Mars* (eds H. Kieffer, H., Jakosky, B., Snyder, C. & M. Matthews) 1180–1220 (Univ. Arizona Press, Tucson, 1992).
23. Ward, W. R. in *Mars* (eds Kieffer, H. H., Jakosky, B., Snyder, C. & Matthews, M. S) 298–320 (Univ. Arizona Press, Tucson 1992).
24. Cutts, J. A. & Lewis, B. H. Models of climate cycles recorded in Martian polar layered deposits. *Icarus* **50,** 216–244 (1982).

Acknowledgements

E. Jensen, M. Roth, M. Ryan, D. Sharman and J. Warren provided technical assistance. This work was supported in part by NASA.

Correspondence and requests for materials should be addressed to P.C.T. (e-mail: thomas@cuspif.tn.cornell.edu).

Impossibility of deleting an unknown quantum state

Arun Kumar Pati*† & Samuel L. Braunstein*

* *Quantum Optics and Information Group, Informatics, Dean Street, University of Wales, Bangor LL57 1UT, UK*
† *Theoretical Physics Division, BARC, Bombay 400 085, India*

A photon in an arbitrary polarization state cannot be cloned perfectly[1,2]. But suppose that at our disposal we have several copies of a photon in an unknown state. Is it possible to delete the information content of one or more of these photons by a physical process? Specifically, if two photons are in the same initial polarization state, is there a mechanism that produces one photon in the same initial state and the other in some standard polarization state? If this could be done, then one would create a standard blank state onto which one could copy an unknown state approximately, by deterministic cloning[3,4] or exactly, by probabilistic cloning[5,6]. This could in principle be useful in quantum computation, where one could store new information in an already computed state by deleting the old information. Here we show, however, that the linearity of quantum theory does not allow us to delete a copy of an arbitrary quantum state perfectly. Though in a classical computer information can be deleted (reversibly) against a copy[7], the analogous task cannot be accomplished, even irreversibly, with quantum information.

Quantum information has the unique property that it cannot be amplified accurately. If an arbitrary state could be cloned, then by using non-local resources one could send signals faster than light[1,2]. However, orthogonal quantum states can be perfectly copied. Although two non-orthogonal photon-states cannot be copied perfectly by a unitary process[8], they can be copied by a unitary-reduction process[5]. More interestingly, non-orthogonal states